RSC Advances

PAPER

View Article Online
View Journal | View Issue

Cite this: *RSC Adv.*, 2019, **9**, 2645

Strain-effected physical properties of ferromagnetic insulating $La_{0.88}Sr_{0.12}MnO_3$ thin films

Younghak Kim, †*[a] Sangkyun Ryu†[b] and Hyoungjeen Jeen [b]

Received 30th November 2018
Accepted 11th January 2019

DOI: 10.1039/c8ra09851d

rsc.li/rsc-advances

The functional perovskite $La_{1-x}Sr_xMnO_3$ (LSMO) possesses various exotic phases owing to competing physical parameters and internal degrees of freedom. In particular, the nature of the ferromagnetic insulating phase (FMI) has not been adequately explored, resulting in a limited understanding of the relationship between crystal structure and magnetism. To investigate this structure–property relationship, epitaxial $La_{0.88}Sr_{0.12}MnO_3$ thin films were grown on two different substrates, (001) $SrTiO_3$ and (001) $(LaAlO_3)_{0.3}(Sr_2AlTaO_6)_{0.7}$, by pulsed laser deposition. Element-specific and surface-sensitive techniques were applied in conjunction with bulk magnetometry to investigate the inextricable link between the structures and magnetic properties of the films and the effects of tuning the strain. The results unambiguously demonstrate that structure–property relationship of a FMI LSMO tuned by strain has a crucial role for manipulating the properties in the FMI regime.

Introduction

$La_{1-x}Sr_xMnO_3$ (LSMO) has attracted considerable attention over recent years due to not only its exotic chemical and physical properties in various complex phases but also its great potential for a variety of applications. LSMO is widely regarded as a useful material in practical areas such as spintronics and energy device materials because the perovskite manganite structure results in the colossal magnetoresistance (CMR) effect and half-metal properties with potential application to magnetic memory devices.[1,2] Furthermore, some hole-doped LSMO materials exhibit high Curie temperatures (T_c) above room temperature.[3] LSMO also possesses a high conductivity and good thermal expansion coefficient, making it a suitable cathode material for commercial solid oxide fuel cells (SOFCs).[4,5] In addition, the Jahn–Teller (JT) distortion forms polarons above the T_c ($\approx$370 K), as changing the electronic and atomic structures is associated with the conductivity of materials.[6] With respect to physical properties, the complex phases of hole-doped manganites have numerous different ground states caused by competing internal degrees of freedom and applied parameters such as temperature, electric field, magnetic field, and strain.[7,8] The exotic phases include various magnetic and electronic phases, a hole-doping metal–insulator transition, and a Griffiths phase.[3,9,10]

LSMO has complex electronic and magnetic ground states such as the paramagnetic insulating (PMI) phase, ferromagnetic metallic (FMM) phase, and ferromagnetic insulating (FMI) phase.[11,12] In particular, the nature of the FMI phase is not well understood compared with that of the FMM phase, which can be described using the double-exchange model. Furthermore, the relationships between the applied parameters and the resulting magnetic states are not yet well established. To further investigate the FMI phase of $La_{1-x}Sr_xMnO_3$, the low-doping region ($x \leq 0.15$) is interesting since the exotic FMI phase is stabilized under these conditions. Thus, this material represents a very attractive model for exploring the correlation between the crystal structure and magnetism.

In an effort to elucidate the interplay between the crystal structure and magnetism of perovskite oxides, numerous studies have investigated the thickness dependence of the structural, electrical, and magnetic properties of epitaxial thin films such as $BiFeO_3$, $LiFe_5O_8$, and $La_{1-x}Sr_xMnO_3$.[13–16] However, the FMI phase of $La_{0.88}Sr_{0.12}MnO_3$ has not been adequately investigated. Few studies were conducted partially with transport measurements.[11,17]

In this work, we report on the exotic magnetic properties caused by substrate-effected strain from two distinct substrates with various experimental methods. Since the applied parameters can be conveniently used to tune the physical properties such as crystallographic structure and magnetism of epitaxial LSMO thin films,[6,7] we performed structural characterization, X-ray spectroscopy, and magnetic measurements to observe the effects of substrate-effected strain on the films.

[a]*Pohang Accelerator Laboratory, Pohang University of Science and Technology, Pohang 37673, Korea. E-mail: iyhkim@postech.ac.kr*

[b]*Department of Physics, Pusan National University, Busan, 46241, Korea*

† These authors contributed equally to this work.

Experimental

Sample preparation

Lightly doped manganite $La_{0.88}Sr_{0.12}MnO_3$ belongs to the space group *Pbnm* and its lattice parameters are $a = 5.5425$ Å, $b = 5.5346$ Å, and $c = 7.7857$ Å.[18] We grew epitaxial thin films of (001) orthorhombic $La_{0.88}Sr_{0.12}MnO_3$ on cubic (001) $SrTiO_3$ (STO, $a = 3.905$ Å) and $(LaAlO_3)_{0.3}(Sr_2AlTaO_6)_{0.7}$ (LSAT, $a = 3.868$ Å) single-crystal substrates by pulsed laser deposition (Q-switched pulsed Nd:YAG laser with $\lambda = 355$ nm). The laser fluence was 0.62 J cm^{-2}. We used a $La_{0.88}Sr_{0.12}MnO_3$ target from Toshima, Japan. The growth conditions were 600 °C at 100 mTorr of an oxygen partial pressure. We also optimized the growth process by using a 300 Torr oxygen partial pressure to remove oxygen vacancies upon cooling.

Characterization of thin films

To examine the crystal structural properties of the epitaxial LSMO thin films deposited on single-crystal STO and LSAT substrates, we performed X-ray reflectivity (XRR) and X-ray diffraction (XRD) measurements with a wavelength (λ) of 1.54 Å using a high-resolution X-ray diffractometer (HR-XRD, SmartLab, Rigaku). Fig. 1(a) and (b) show the XRR patterns for the epitaxial LSMO/STO and LSMO/LSAT films, respectively. The results revealed a well-defined film thickness of 17 nm on STO and 18 nm on LSAT, allowing a reasonable comparison to be made between the two films owing to their similar thickness. Fig. 1(c) and (d) show the XRD patterns, which clearly demonstrated that the films were epitaxial and free from impurities. Since the crystal structure of LSMO is orthorhombic, based on a pseudocubic model, the lattice constant for an LSMO thin film is 3.916 Å. As the lattice constants of the substrates are 3.905 Å for STO and 3.868 Å for LSAT, the lattice mismatches were

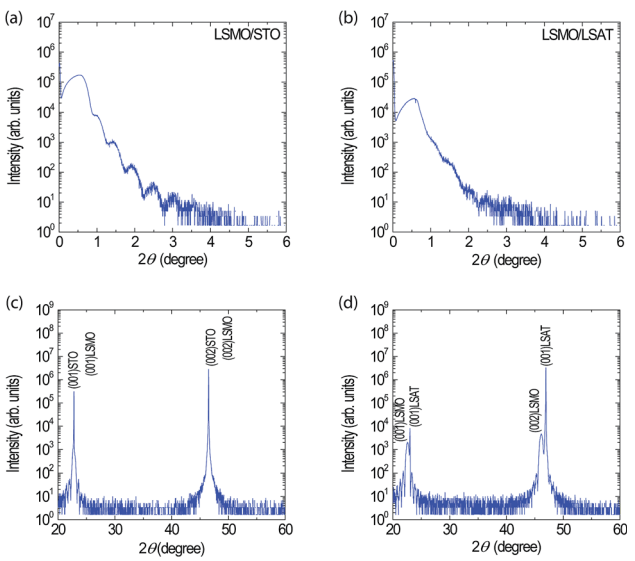

Fig. 1 XRR patterns of the epitaxial thin films of (a) LSMO/STO and (b) LSMO/LSAT. θ–2θ XRD patterns of the epitaxial thin films of (c) LSMO/STO and (d) LSMO/LSAT. These results confirm the successful growth of uniform thin films.

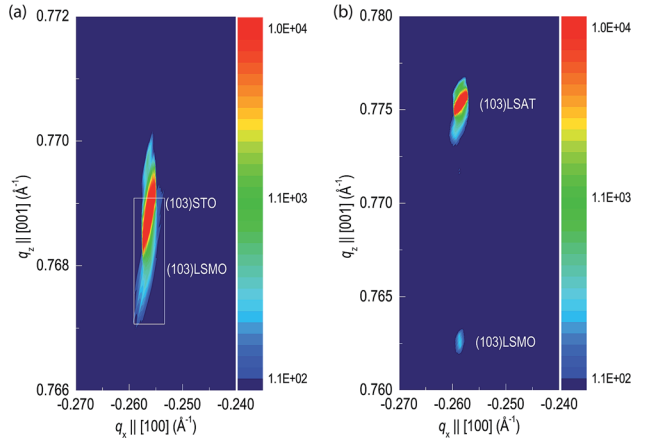

Fig. 2 RSM images for the (a) (103) STO substrate and (b) (103) LSAT substrate. The square box in (a) is a guide to the eye for LSMO. These contour maps confirm the presence of strain in the films.

−0.28% for LSMO/STO and −1.24% for LSMO/LSAT, where the negative sign indicates compressive strain.

To confirm the existence of substrate-effected strain in the LSMO films, we used the reciprocal space mapping (RSM) method. The RSM measurements were performed for the (103) STO and (103) LSAT substrates. Fig. 2(a) and (b) show the corresponding RSM images. The results clearly confirmed that the epitaxial LSMO films exhibited the same in-plane lattice constants for each substrate, indicating the presence of compressive substrate-effected strain in the epitaxial thin films.

Results and discussion

The temperature and field dependences of the magnetization were measured using a superconducting quantum interference device (SQUID) magnetometer. We used an applied magnetic field of 100 Oe and field cooling to clearly observe the T_c in the temperature dependence of magnetization (M–T) curves for the epitaxial LSMO/LSAT and LSMO/STO thin films. The applied magnetic field is perpendicularly to the plane of thin films. Fig. 3(a) shows that the T_c values were 170 K and 190 K for the LSMO/LSAT and LSMO/STO films, respectively. It should be noted that an anomaly of magnetization was observed for the LSMO/LSAT film, in that the magnetization initially increased up to ~106 K and thereafter decreased. The low temperature behavior of LSMO on LSAT is reminding us of spin glass and/or cluster glass.[19] However, in this work, we have focused on biaxial substrate-induced strain effect on magnetism. This indicates that charge-orbital ordering (COO) occurred in this film.[20] Since the in-plane compressive strain reduces the bond distance of Mn^{3+}–O^{2-}–Mn^{4+} by stretching the MnO_6 octahedra in the out-of-plane direction, the value of T_c decreases owing to the stronger double exchange.[21] Furthermore, elongation of the MnO_6 octahedra also stimulate the competition of the internal degrees of freedom and shift the T_c to a lower temperature. This is caused by the stabilization of the $d_{3z_2-r_2}$ with reduced

ferromagnetic interaction in the *ab* plane since T_c links inextricably to delocalize the e_g orbitals.[17,21]

Fig. 3(b) shows the magnetization as a function of the applied field (*M*–*H* hysteresis loops), which was measured at 80 K in the fully FMI phase for both substrates below their T_c. These loops revealed distinct differences in the saturated magnetic moments (M_s) of the two films. The magnetization of the epitaxial LSMO thin film grown on STO was smaller than that of the LSMO film grown on LSAT. This implies that a greater compressive strain leads to a higher M_s. This means that the in-plane compressive strain can control magnetic properties. It should also be noted that, as shown in the inset of Fig. 3(b), the coercive field was higher for LSMO/LSAT than for LSMO/STO. This may also be the result of the complex competition between the COO and JT interactions.

We also measured resistivity as a function of temperature as shown Fig. 3(c). These curves indicate that the thin films show indeed insulator behavior. Also, note that there are little humps, pointed by arrows, around 170 K on LSMO/LSAT and 190 K around on LSMO/STO. These present that there is the ferromagnetic phase transition which agrees well to the result of magnetization measurements in terms of temperature shown in Fig. 3(a).

To examine the influence of the substrate-effected strain on the magnetic properties of the films, we performed X-ray magnetic circular dichroism (XMCD) with X-ray absorption spectroscopy (XAS) on the 2A beamline of Pohang Accelerator Laboratory. The XAS and XMCD spectra were obtained in total electron yield mode using an elliptically polarized undulator. XAS and XMCD are very powerful techniques for studying the electronic and magnetic structures of transition-metal materials owing to their element-specific excitation.[22,23] XAS provides direct information concerning the valence states of transition-metal materials such as Mn ions, because the core electrons in the 2p orbitals are excited to the 3d orbitals upon absorption.[22] XMCD is a unique tool for separately determining the spin and orbital magnetic moments for the element-specific moment.[24–26]

For these experiments, the base pressure of the experimental chamber was maintained below 5×10^{-10} Torr during the measurements. The applied temperature was 80 K for consistency with the *M*–*H* measurements. To obtain the XMCD spectra, an external magnetic field of $H \approx 0.7$ T was applied in the out-of-plane direction of the sample. The applied filed direction is the same to the SQUID measurement. The field was flipped to be parallel (μ_+) and antiparallel (μ_-) to the circularly polarized photon helicity.[25,27] Then, the dichroism ($\Delta\mu = \mu_+ - \mu_-$) was calculated from the difference between the two values at each data point. The XAS spectra were normalized for comparison of the XMCD results. Fig. 4 presents the obtained Mn $L_{2,3}$-edge spectra of the FMl LSMO thin films on the two substrates, illustrating the XAS and XMCD spectra of the Mn ions in the LSMO/STO and LSMO/LSAT thin films. From the XAS results, Mn L_3-edge spectra are roughly 641.95 eV. This confirms that our samples were well grown as $La_{0.88}Sr_{0.12}MnO_3$ since the *x* of Sr in the thin films is 0.12 in good agreement with the spectra of various Sr concentrations studied by Abbate *et al.*[23]

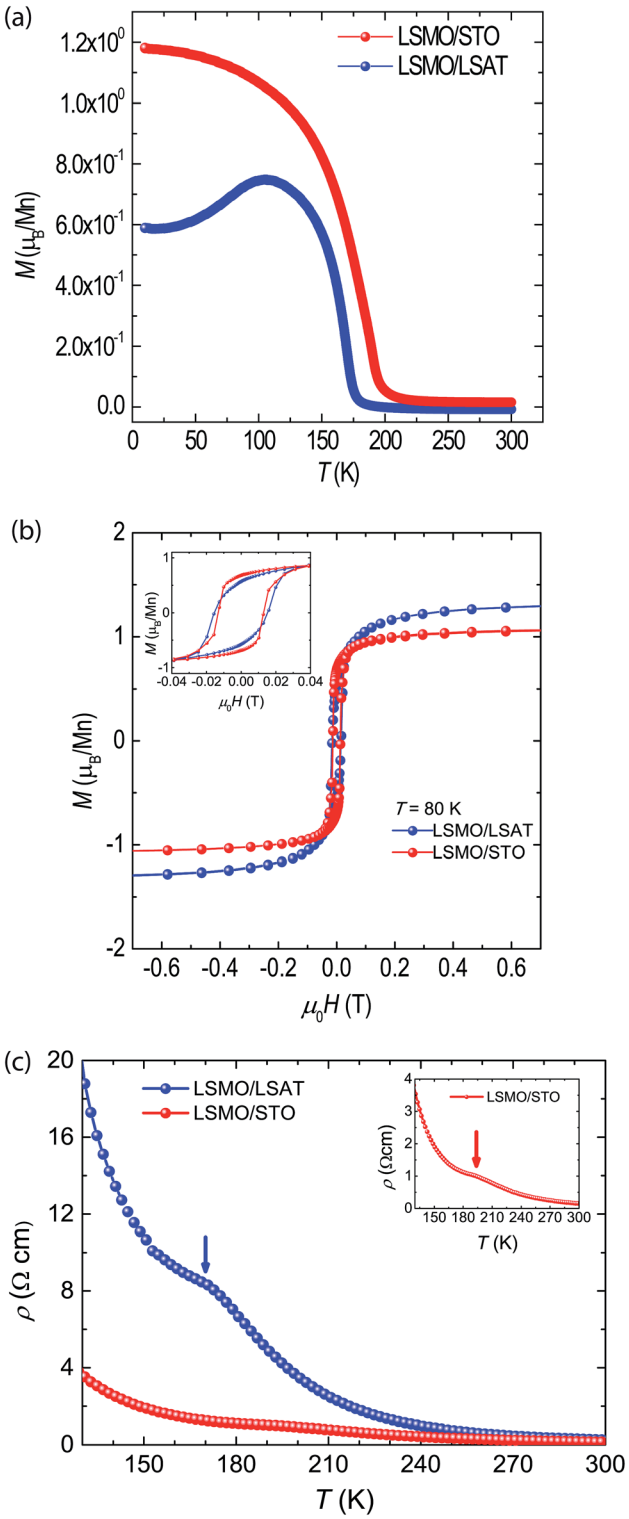

Fig. 3 (a) Magnetization curves as a function of temperature, obtained at an applied magnetic field of 100 Oe. COO occurred in the epitaxial LSMO/LSAT thin film, as revealed by the anomalous increase in magnetization up to ~106 K and subsequent decrease, which was not observed for the epitaxial LSMO/STO thin film. (b) Magnetic hysteresis loops of the LSMO films under different in-plane compressive strains at 80 K. The magnetization of LSMO/LSAT is greater than that of LSMO/STO, which implies that increased compressive strain reduces the magnetization. (c) Resistivity *vs.* temperature curves of LSMO thin films.

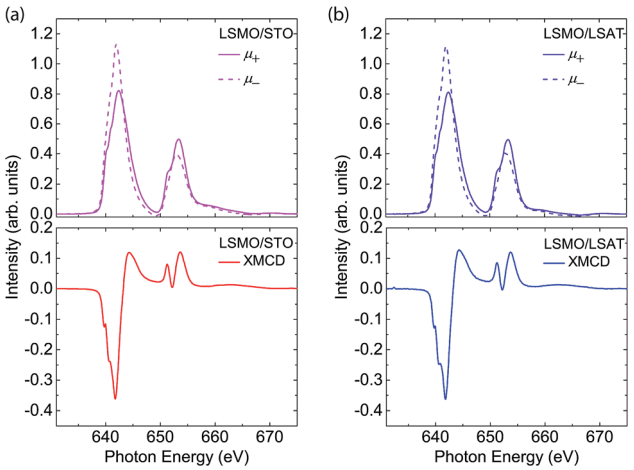

Fig. 4 Mn $L_{2,3}$-edge XAS and XMCD spectra of the epitaxial thin films of (a) LSMO/STO and (b) LSMO/LSAT. The XAS spectra were normalized to allow easier comparison of the XMCD results for the two samples. The dichroism is $\Delta\mu = \mu_+ - \mu_-$. Both spectra were recorded at 80 K in the presence of an external magnetic field of approximately 0.7 T.

According to the XMCD sum rules, the spin magnetic moment M_{spin} and orbital magnetic moment M_{orb} can be expressed as follows:[24–26]

$$M_{spin} = -\frac{6p - 4q}{r} \times (10 - n_{3d}) \left(1 + \frac{7\langle T_z \rangle}{2\langle S_z \rangle}\right)^{-1}, \quad (1)$$

$$M_{orb} = -\frac{4q}{3r} \times (10 - n_{3d}). \quad (2)$$

where
$p = \int_{L_3} \Delta\mu dE, q = \int_{L_3+L_2} \Delta\mu dE$, and $r = \int_{L_3+L_2} (\mu_+ + \mu_-) dE$.

L_3 and L_2 are the integration range, and n_{3d} is the occupation number of 3d electrons in a Mn ion. The $\langle T_z \rangle / \langle S_z \rangle$ term can be neglected in this analysis.[24,25] Here, we select $n_{3d} = 4$ since Mn^{3+} is the dominant ion influencing the magnetic structure in $La_{0.88}Sr_{0.12}MnO_3$ films. For the LSMO/STO film, M_{spin} and M_{orb} were estimated to be 1.44 μ_B/Mn and -1.71×10^{-2} μ_B/Mn, respectively. These give $M_{orb}/M_{spin} = -1.19 \times 10^{-2}$. For the LSMO/LSAT film, M_{spin} and M_{orb} were estimated to be 1.50 μ_B/Mn and -1.51×10^{-2} μ_B/Mn, respectively. These give $M_{orb}/M_{spin} = -1.01 \times 10^{-2}$. The negative sign indicates that the spin and orbital moments are antiparallel to each other as a result of Hund's rule. The spin magnetic moments are comparable to the results of the *M–H* measurements and in the same order as expected. The M_s values were approximately 1.06 μ_B/Mn for the LSMO/STO film and 1.29 μ_B/Mn for the LSMO/LSAT film. These are summarized in Table 1.

As demonstrated by the XMCD results, the different spin magnetic moments of the Mn ions on the two substrates correspond to the degree of compressive strain effected by the substrates. These are in good agreement with the SQUID results. With a bulk measurement of SQUID, the results of XMCD supports strongly to the structure–property relationship. Unlike the FMM of LSMO, the FMI cannot be explained simply by using the double-exchange interaction, as mentioned earlier in the text. Instead, the situation is more complicated as the long-range COO must be considered, since an epitaxial $La_{0.88}Sr_{0.12}MnO_3$ film on a substrate is a lightly doped manganite with lattice distortion.[11,20] Previous studies reported that the COO of lightly doped $La_{1-x}Sr_xMnO_3$ is associated with lattice distortion and the result of a complex interplay between electron–electron correlation, double exchange, and JT distortion in the Mn^{3+}–O^{2-}–Mn^{4+} bond.[11,12,20,28] This can apply to our material model in this work. The orbital configuration associated with the electronic structure is related to the competition between these factors in the FMI phase. This causes a change in the magnetic structure of the epitaxial thin film. Thus, our results indicate that a large compressive strain effected by a substrate presents the COO transition with the JT distortion and the structure deformation. Like the *M–H* curves shown in Fig. 3(b), the XMCD results similarly demonstrated that the M_{spin} of the LSMO/LSAT thin film was larger than that of the LSMO/STO film. In contrast, the opposite was true for the orbital magnetic moments, where the M_{orb} of LSMO/LSAT was smaller than that of LSMO/STO (Table 1). A large in-plane compressive strain gives rise to distortion of the MnO_6 octahedra, resulting in different magnetic properties.

Consequently, this implies that a large compressive strain can afford unconventional properties with the electron configuration dependent on the complex interactions between the COO, JT distortion, and structural deformation. The consistent experimental results obtained from the bulk measurements and the surface-sensitive techniques support the idea that lattice distortion is intrinsically linked to magnetism in the FMI phase of $La_{0.88}Sr_{0.12}MnO_3$ as a result of the complex interactions discussed above.

Conclusions

In summary, we have used X-ray spectroscopy and magnetic measurements to examine the magnetic structures of FMI $La_{0.88}Sr_{0.12}MnO_3$ thin films, which are a potential model for the

Table 1 Comparison of the lattice mismatches, spin magnetic moments, and orbital magnetic moments for the LSMO/STO and LSMO/LSAT thin films. The spin and orbital magnetic moments were calculated from the XMCD results (Mn^{3+} ions; $n_{3d} = 4$) for each epitaxial thin film. The negative sign of the mismatch indicates that the films were subjected to in-plane compressive strain. The M_s values were obtained from the SQUID measurements

	Lattice mismatch	M_s (μ_B/Mn)	M_{spin} (μ_B/Mn)	M_{orb} (μ_B/Mn)	M_{orb}/M_{spin}
LSMO/STO	−0.28%	1.06	1.44	-1.71×10^{-2}	-1.19×10^{-2}
LSMO/LSAT	−1.24%	1.29	1.50	-1.51×10^{-2}	-1.01×10^{-2}

FMI phase of LSMO at low temperature. The structural deformation of the epitaxial thin films grown on two different substrates effected changes in the magnetic properties. Our results indicate an inextricable link between crystal structure and physical properties, particularly magnetic properties. In the epitaxial LSMO thin films, a large compressive strain caused displacement of the MnO_6 octahedra in the out-of-plane direction and suppressed it in the in-plane direction. Distortion of the MnO_6 octahedra influenced the double-exchange interaction in Mn^{3+}–O^{2-}–Mn^{4+} *via* a complex interplay with COO and JT distortion. This structural deformation links degrees of freedom such as spin, charge, and orbital in the lightly doped $La_{1-x}Sr_xMnO_3$. The correlation between the structural, electrical, and magnetic properties can be explained by the competition between the COO, JT distortion, and double-exchange interaction. This study provides an opportunity to improve our understanding of the nature of the FMI phase of lightly doped $La_{1-x}Sr_xMnO_3$ by exploiting the advantages of XMCD, a surface-sensitive technique. It suggests that further intensive study of a FMI LSMO will contribute to enhance our understanding of exotic physical and chemical properties in the regime for great potential applications.

Conflicts of interest

There are no conflicts to declare.

Acknowledgements

This research was supported by the Basic Science Research Program through the National Research Foundation of Korea (NRF), funded by the Ministry of Education (NRF-2018R1D1A1B07046980). H. J. J. and S. K. R. were supported by NRF Korea (2017K1A3A7A09016305).

Notes and references

1 A. P. Ramirez, *J. Phys.: Condens. Matter*, 1997, **9**, 8171.
2 J.-H. Park, E. Vescovo, H.-J. Kim, C. Kwon, R. Ramesh and T. Venkatesan, *Nature*, 1998, **392**, 794.
3 A. Urushibara, Y. Moritomo, T. Arima, A. Asamitsu, G. Kido and Y. Tokura, *Phys. Rev. B: Condens. Matter Mater. Phys.*, 1995, **51**, 14103.
4 S. P. Jiang, *J. Mater. Sci.*, 2008, **43**, 6799.
5 J. Sacanell, J. H. Sánchez, A. E. R. López, H. Martinelli, J. Siepe, A. G. Leyva, V. Ferrari, D. Juan, M. Pruneda, A. M. Gómez and D. G. Lamas, *J. Phys. Chem. C*, 2017, **121**, 6533.
6 N. Mannella, A. Rosenhahn, C. H. Booth, S. Marchesini, B. S. Mun, S.-H. Yang, K. Ibrahim, Y. Tomioka and C. S. Fadley, *Phys. Rev. Lett.*, 2004, **92**, 166401.
7 M. B. Salamon and M. Jaime, *Rev. Mod. Phys.*, 2001, **73**, 583.
8 M. Uehara, S. Mori, C. H. Chen and S. W. Cheong, *Nature*, 1999, **399**, 560.
9 J. Deisenhofer, D. Braak, H.-A. Krug von Nidda, J. Hemberger, R. M. Eremina, V. A. Ivanshin, A. M. Balbashov, G. Jug, A. Loidl, T. Kimura and Y. Tokura, *Phys. Rev. Lett.*, 2005, **95**, 257202.
10 M. Paraskevopoulos, F. Mayr, J. Hemberger, A. Loidl, R. Heichele, D. Maurer, V. Müller, A. A. Mukhin and A. M. Balbashov, *J. Phys.: Condens. Matter*, 2000, **12**, 3993.
11 Y. Endoh, K. Hirota, S. Ishihara, S. Okamoto, Y. Murakami, A. Nishizawa, T. Fukuda, H. Kimura, H. Nojiri, K. Kaneko and S. Maekawa, *Phys. Rev. Lett.*, 1999, **82**, 4328.
12 H. Nojiri, K. Kaneko, M. Motokawa, K. Hirota, Y. Endoh and K. Takahashi, *Phys. Rev. B: Condens. Matter Mater. Phys.*, 1999, **60**, 4142.
13 D. S. Rana, K. Takahashi, K. R. Mavani, I. Kawayama, H. Murakami, M. Tonouchi, T. Yanagida, H. Tanaka and T. Kawai, *Phys. Rev. B: Condens. Matter Mater. Phys.*, 2007, **75**, 060405.
14 R. Prasad, H. K. Singh, M. P. Singh, W. Prellier, P. K. Siwach and A. Kaur, *J. Appl. Phys.*, 2008, **103**, 083906.
15 R. Zhang, M. Liu, L. Lu, S.-B. Mi and H. Wang, *J. Mater. Chem.*, 2015, **3**, 5598.
16 P. Dey, T. K. Nath and A. Taraphder, *Appl. Phys. Lett.*, 2007, **91**, 012511.
17 L. Hu, Z. Sheng, X. Hu, R. Zhang, B. Wang, W. Song and Y. Sun, *J. Phys. D: Appl. Phys.*, 2012, **45**, 175002.
18 D. E. Cox, T. Iglesias, E. Moshopoulou, K. Hirota, K. Takahashi and Y. Endoh, *Phys. Rev. B: Condens. Matter Mater. Phys.*, 2001, **64**, 024431.
19 E. Dagotto, *New J. Phys.*, 2005, **7**, 67.
20 B. Dabrowski, X. Xiong, Z. Bukowski, R. Dybzinski, P. W. Klamut, J. E. Siewenie, O. Chmaissem, J. Shaffer, C. W. Kimball, J. D. Jorgensen and S. Short, *Phys. Rev. B: Condens. Matter Mater. Phys.*, 1999, **60**, 7006.
21 A. Sadoc, B. Mercey, C. Simon, D. Grebille, W. Prellier and M.-B. Lepetit, *Phys. Rev. Lett.*, 2010, **104**, 046804.
22 F. M. F. de Groot, J. C. Fuggle, B. T. Thole and G. A. Sawatzky, *Phys. Rev. B: Condens. Matter Mater. Phys.*, 1990, **42**, 5459.
23 M. Abbate, F. M. F. de Groot, J. C. Fuggle, A. Fujimori, O. Strebel, F. Lopez, M. Domke, G. Kaindl, G. A. Sawatzky, M. Takano, Y. Takeda, H. Eisaki and S. Uchida, *Phys. Rev. B: Condens. Matter Mater. Phys.*, 1992, **46**, 4511.
24 B. T. Thole, P. Carra, F. Sette and G. van der Laan, *Phys. Rev. Lett.*, 1992, **68**, 1943.
25 C. T. Chen, Y. U. Idzerda, H.-J. Lin, N. V. Smith, G. Meigs, E. Chaban, G. H. Ho, E. Pellegrin and F. Sette, *Phys. Rev. Lett.*, 1995, **75**, 152.
26 Y. Teramura, A. Tanaka, B. T. Thole and T. Jo, *J. Phys. Soc. Jpn.*, 1996, **65**, 3056.
27 J.-Y. Kim, T. Y. Koo and J.-H. Park, *Phys. Rev. Lett.*, 2006, **96**, 047205.
28 S. Uhlenbruck, R. Teipen, R. Klingeler, B. Büchner, O. Friedt, M. Hücker, H. Kierspel, T. Niemöller, L. Pinsard, A. Revcolevschi and R. Gross, *Phys. Rev. Lett.*, 1999, **82**, 185.